Tau inhibits the long-range, dynein-mediated motility of early phagosomes

Daniel Beaudet[a], Christopher L. Berger[b], Adam G. Hendricks[a]*

[a]Department of Bioengineering, McGill University, Montreal, QC, Canada, H2X 3X8

[b]Department of Molecular Physiology and Biophysics, University of Vermont, Burlington, VT

*Corresponding Author: adam.hendricks@mcgill.ca

Abstract

Microtubule-associated proteins (MAPs) regulate the teams of kinesin and dynein motors that transport organelles. Tau is a neuronal MAP that organizes the axonal cytoskeleton and its misregulation is linked to defective axonal transport and neurodegenerative disease. We reconstituted the motility of endocytic organelles along microtubules *in vitro* to ask how the sets of motors transporting a cargo determine its motility and response to tau. Here, we show that early phagosomes (EPs) primarily undergo unidirectional retrograde transport while late phagosomes (LPs) move bidirectionally. Accordingly, EPs and LPs are bound by different numbers and combinations of kinesin-1, kinesin-2, kinesin-3, and dynein. From our previous studies showing that tau biases the transport of LPs towards the microtubule minus-end, we expected that minus-end directed EPs would be less sensitive to tau. Instead, here we find that tau strongly inhibits long-range dynein-mediated EP motility. Tau reduces the magnitude of the forces exerted on EPs in both directions along microtubules. Dynein is the dominant motor in EP transport, and tau strongly impedes forces generated by teams of multiple dynein motors and accelerates dynein unbinding under load. Our data indicate that tau inhibits the minus-end directed transport of EPs by reducing the number of dynein motors engaged along microtubules. These results are surprising, as previous single-molecule studies showed that dynein is less sensitive to tau compared to kinesin. Our results show that specific cargoes differentially respond to tau, where dynein-complexes on EPs are more sensitive to tau inhibition than those that transport LPs.

Keywords: Tau, microtubule associated proteins, kinesin, dynein, organelle transport.

Introduction

Motor-mediated transport is essential for the spatial and functional distribution of organelles and vesicular cargoes in cells. Kinesins -1, -2, and -3 are the principal plus-end directed microtubule-based motors that drive anterograde transport, while cytoplasmic dynein drives minus-end directed retrograde transport (Hirokawa et al., 2010; Reck-Peterson et al., 2018). Cargoes bound simultaneously by kinesin and dynein move bidirectionally along microtubules, which enables them to navigate around obstacles and achieve long-range targeted trafficking throughout the crowded cellular environment (Gross et al., 2002; Welte, 2004; Hendricks et al., 2010; Chaudhary et al., 2018). Intracellular cargoes exhibit diverse motility due to differences in their sets of kinesin and dynein motors as well as the mechanisms that coordinate their opposing activity. For instance, early endosomes are bound by kinesin-1, kinesin-3, and dynein and typically exhibit short bursts of unidirectional motility (Brown et al., 2005; Hoepfner et al., 2005; Loubéry et al., 2008; Flores-Rodriguez et al., 2011). In filamentous fungi, early endosomes are driven by tightly bound kinesin-3 motors, and the transient binding of dynein causes their directionality to switch between long-range anterograde and retrograde transport (Schuster et al., 2011). Whereas late endosomes and lysosomes simultaneously associate with members of the kinesin-1, -2, -3 families and dynein and exhibit robust bidirectional transport (Matsushita et al., 2004; Brown et al., 2005; Loubéry et al., 2008; Rosa-Ferreira and Munro, 2011; Pu et al., 2016). Multiple types of kinesins on the same cargo could be required for different organelle functions or target organelles to different destinations by controlling the activity of specific kinesins or through their selective transport along microtubules with different posttranslational modifications (Guardia et al., 2016; Pu et al., 2016). Although many kinesin-cargo interactions have been identified (Jenkins et al., 2012; Bentley et al., 2015; Hummel and Hoogenraad, 2021), determining the full complement of native motors on most endogenous cargoes, and how these sets of motors are regulated to achieve targeted trafficking remains a challenging problem.

Microtubule tracks spatially regulate trafficking in cells. Microtubule associated proteins (MAPs) organize the cytoskeleton by controlling the polarity, bundling, and stability of microtubules, as well as the interactions and movement of motor proteins along them (Liu et al., 2012; Lipka et al., 2016; Gumy et al., 2017; Balabanian et al., 2017; Chaudhary et al., 2018; Harterink et al., 2018; Chaudhary et al., 2019; Hooikaas et al., 2019; Ferro et al., 2022). Several MAPs act as regulators of motor proteins. One of the most well-studied is the neuronal MAP tau, which is implicated in Alzheimer's Disease and related neurodegenerative diseases collectively known as tauopathies. Pathogenic forms of tau perturb the organization of the axonal cytoskeleton and lead to synaptic disfunction and neuronal dystrophy (Mandelkow et al., 2003). Despite the link between aberrant tau regulation and neuropathology, it remains unclear what role tau plays in regulating axonal transport in healthy neurons and how defects lead to neurodegeneration.

Single-molecule studies show that microtubule motors have varying sensitivities to tau. Tau strongly reduces the processivity and landing rates of kinesin-1 and kinesin-3 along microtubules *in vitro* (Vershinin et al., 2007; Dixit et al., 2008; McVicker et al., 2011; Monroy et al., 2018). In contrast, kinesin-2 is less processive, but is better able to navigate around tau due to its longer more flexible neck linker domain (Hoeprich et al., 2014; Hoeprich et al., 2017). Dynein is also less sensitive than kinesin-1 and often passes through or reverses directions upon encountering tau patches (Dixit et al., 2008; Vershinin et al., 2008; Tan et al., 2019). In addition, there are multiple isoforms of tau expressed throughout the adult brain that have different impacts on the motility of motor proteins. The 3RS-tau isoform strongly inhibits kinesin-1 and dynein processivity compared to 4RL-tau (Vershinin et al., 2007; Dixit et al., 2008; Vershinin et al., 2008; McVicker et al., 2011). This is likely because the 3RS-tau isoform binds

more statically along microtubules and has a higher propensity to form patches compared to 4RL-tau (Hinrichs et al., 2012; McVicker et al., 2014). Tau patch formation is a potential regulatory mechanism to selectively govern the accessibility of the microtubule surface for motors and other MAPs (Tan et al., 2019; Siahaan et al., 2019). Conversely, patches or larger-order tau-complexes that form along microtubules could also act as precursors to neurofibrillary tangles found in neurodegenerative disease (Gyparaki et al., 2021). Taken together, these studies show that tau functions as a selective barrier along the microtubule lattice that allows some types of motors to pass through while impeding others. However, endogenous cargoes are often transported by teams of multiple kinesins and dynein, and it is less clear how these heterogenous teams of motors are regulated by tau.

MAPs decorate the microtubules that serve as tracks for many types of cargoes, leading us to ask how MAPs might target specific cargoes to different destinations in the cell. To address this question, we characterized the sets of motors bound to endocytic cargoes and used *in vitro* reconstitution to test the impact of 3RS-tau on their motility along microtubules. We found that the type and number of motors on a cargo determines its response to tau regulation. In cells, early phagosomes (EPs) are unidirectional and more often transported towards the microtubule minus-end, whereas late phagosomes (LPs) move bidirectionally. EPs were bound by more kinesin-1 and kinesin-3 but had fewer kinesin-2 and dynein compared to LPs. In addition, LPs were more frequently bound by all three motors compared to EPs, which associate with more heterogeneous complements of motors. Our previous work showed that isolated LPs move bidirectionally *in vitro* and tau biases their motility towards the minus-end of microtubules (Chaudhary et al., 2018). Here we show that tau more strongly inhibits EP motility. Tau reduced the number of long-range minus-end directed events but had less of an inhibitory effect on short minus-end runs or plus-end directed runs. In addition, we showed that tau reduced the overall magnitude of forces exerted by EPs with the highest reduction of forces generated by teams of multiple dynein motors. These results suggest that differences in the number and type of motors present on cargoes govern their movement and their response to tau. Thus, tau directs the transport of different cargoes by selectively tuning the motility and forces exerted by kinesin and dynein teams.

Results

EPs and LPs move differently and are transported by different sets of motors

We first sought to determine how the sets of motors that associate with different cargoes correlate with their motility. To test this, we analyzed phagosomes at different stages of maturation. Latex bead-containing phagosomes are a powerful system to examine how the membrane composition, biochemical properties, and ensembles of motors transporting endocytic organelles change in response to maturation and fusion events (Desjardins et al., 1994a; Desjardins et al., 1994b; Garin et al., 2001; Goyette et al., 2012; Blocker et al., 1997; Loubéry et al., 2008; Rai et al., 2016). Here, we characterized the motility and quantified the sets of motors on early phagosomes (EPs) and late phagosomes (LPs) from mouse J774A.1 macrophage. To image phagosome motility, cells were treated with 200 nm fluorescent latex beads and the movement of bead-containing phagosomes was monitored using total internal reflection fluorescence (TIRF) microscopy. Time lapse images of EPs were recorded 30–45 minutes after bead uptake and LPs were recorded after 90 minutes. First, we compared the trajectories of EPs and LPs using TrackMate (Tinevez et al., 2017) (Fig 1A) and plotted their displacement to show directionality towards the cell center (microtubule minus-end) or towards the cell periphery (microtubule plus-end) (Fig 1B). EPs had a higher fraction of long-range, minus-end directed trajectories compared to plus-end directed trajectories, while LPs had an

equal fraction of plus-end and minus-end directed trajectories (Fig 1B and C). Phagosomes display stationary, diffusive, and processive periods of motility (Hendricks et al., 2012; Rai et al., 2016). Periods of processive motility were identified as segments of a trajectory between two reversal events with displacements greater than 150 nm, which is consistent with mean-squared displacement (MSD) analysis (Chaudhary et al., 2018). EPs had a higher fraction of long, minus-end directed processive runs and had fewer reversal events compared to LPs (Fig S1A–C). As phagosomes mature, their net motility shifts from minus-end directed, long-range unidirectional transport to bidirectional transport. These results suggest that phagosomes first move towards the perinuclear region of the cell in unidirectional runs, then transition to more bidirectional motility to potentially fuse with other organelles to adopt specialized functions (Goyette et al., 2012; Garin et al., 2001).

The types and numbers of motor proteins that associate with cargoes govern their transport behavior. Previous studies have shown that late phagosomes are transported by teams of kinesin-1, kinesin-2, and dynein (Blocker et al., 1997; Hendricks et al., 2012; Chaudhary et al., 2018). However, it was not clear how the sets of motors bound to phagosomes change in response to maturation. To test this, we quantitatively compared of the number of kinesins-1, -2, -3, and dynein on EPs and LPs. First, we isolated EPs and LPs from cells and performed 3-color immunofluorescence imaging to detect the combination of motors on individual phagosomes. EPs and LPs were isolated from macrophages at 30 or 90 minutes after bead uptake and purified on a sucrose density gradient (Fig 1D). Many LPs (40.7%) were positive for kinesin-1, kinesin-2, and dynein, 21.5% were positive for dynein and either kinesin-1 or kinesin-2, and 8.4% were positive for kinesin-1 and kinesin-2 (Fig 1E–F), in agreement with previous results (Chaudhary et al., 2018). In contrast, the motor sets associated with EPs were more diverse. Only 19.6% of EPs were positive for kinesin-1, kinesin-2, and dynein, 18.8% for kinesin-2 and dynein, 6.1% for kinesin-1 and kinesin-2, and 7.7% for kinesin-1 and dynein (Fig 1E–F). In addition, a higher percentage of EPs (47.8%) were found to have only one type of motor compared to LPs (29.4%) (Fig 1F). Next, we examined if kinesin-3 motors were also present on phagosomes. We tested for kinesin-3 motors separately due limitations in the number of fluorophores that can be used to detect multiple motors within the same experiment. To do this, we co-immunostained EPs and LPs for dynein and the kinesin-3 motors kif16b or kif1b (Fig S2A–B), which have been shown to transport different endocytic organelles (Matsushita et al., 2004; Hoepfner et al., 2005; Blatner et al., 2007). We compared the number of dynein positive phagosomes to the number of phagosomes bound by kinesins -1, -2, and -3 and found that phagosomes are more frequently bound by kinesins-1, -2, and kif16b than kif1b and that EPs are more frequently bound by kif16b than LPs (Fig 1G).

Using stepwise photobleaching analysis, we compared the number of kinesins-1, -2, -3, and dynein motors on EPs and LPs. Isolated phagosomes were immunostained for each motor and imaged using epifluorescence illumination until the fluorescence signal was completely photobleached (Fig S1D). A step-finding algorithm was applied to each intensity trace and used to measure the size and number of steps (Fig S1E–J, S2C–E) (Chen et al., 2014; Chaudhary et al., 2018). Recombinant kinesin-1 (rkin430-GFP) was imaged under similar conditions to determine the number of steps for a single molecule (Fig S1E). We estimated the number of motors present on phagosomes with a positive signal for each motor, and found that 1–4 kinesin-1, 1–6 kinesin-2, and 2–6 dynein bound to EPs, and 1–3 kinesin-1, 2–7 kinesin-2, and 2–8 dynein bound to LPs (Fig 1H), which is consistent with previous findings (Hendricks et al., 2010; Chaudhary et al., 2018; Cella Zanacchi et al., 2019). In addition, we estimated the number of kinesin-3 motors on phagosomes and found that 2–5 kif16b and 1–4 kif1b bound to EPs, and 2–4 kif16b and 1–4 kif1b bound to LPs (Fig 1H). The relative low number of kif1b-positive phagosomes detected suggests that it is not a dominant motor for their transport but

might be required for other specialized functions in cells. EPs associate with fewer dynein and kinesin-2 motors than LPs (Fig 1H). Most LPs were bound by similar sets of opposing motors compared to EPs, which were more heterogeneous and were often bound by single types of motors or different sets of motors (Fig 1E–F, S2A–B). Combined, these results indicate that in contrast to LPs, the types of motors associated with EPs is more variable and EPs often associate with only one or two types of motors at a time. The differences in the numbers and combinations of motors on phagosomes correspond to differences in their motility as they mature in cells, where small changes in the number of engaged motors can result in large changes in their motility (Müller et al., 2008).

Tau reduces minus-end directed early phagosome motility

We next asked how tau regulates the motility of EPs, which are transported by different sets of motors and move differently than LPs. We previously showed that LPs move bidirectionally along microtubules *in vitro* and that tau biases motility towards the microtubule minus-end (Chaudhary et al., 2018). Here, we tested the impact of tau on the motility of EPs under similar conditions. Reconstitution assays were performed using isolated EPs along taxol-stabilized fluorescently labeled microtubules that were polymerized from bright GMPCPP seeds with or without the addition of 10 nM 3RS-tau. Time lapse recordings of EP motility events were imaged using TIRF microscopy and analyzed by subpixel tracking using 2D-Gaussian-fitting (FIESTA) (Ruhnow et al., 2011). Similar to observations in cells, isolated EPs primarily exhibit unidirectional transport in both directions but had a higher fraction of net motion directed toward the minus-end of microtubules (Fig. 2A–B). With tau, the number of long-range minus-end directed EP trajectories was reduced compared to shorter trajectories (< 1 μm) or plus-end directed trajectories (Fig 2C–D). We also noted that the frequency of observable motility events with tau decreased approximately 2-fold, which is likely due to competition for available binding sites between motors and tau (Kellogg et al., 2018). In support, linescans of tau and EP max projections show that EPs often bound and proceeded to move in areas of the microtubule where tau levels were low, which indicates that tau reduced the access of EPs to the microtubule surface (Fig 2E). We also examined how tau impacts the motility of those EPs that bind and move along microtubules and found that 44% of plus-end and 67% of minus-end directed EPs paused when they encountered tau patches, whereas 37% of plus-end and 33% of minus-end directed cargoes passed through tau (Fig 2F). Furthermore, 19% of plus-end directed cargoes detached from microtubules when they encountered tau compared to minus-end directed cargoes that remained attached (Fig 2F).

Isolated EPs exhibit periods of stationary, diffusive, and processive transport, similar to their motility in cells. To determine the contribution of each mode of transport to their overall motility, we segmented trajectories into periods of stationary, diffusive, and processive transport using change point analysis (Fig 3A). Local α-values were calculated using a rolling MSD analysis with a sliding window length of 12 frames (Fig 3A). Change points occurred when the difference between two adjacent α-values was > 0.3. A 'run' was defined as the period of motility between two change points and an α-value of 1 was used as the threshold to determine if a run was diffusive ($\alpha \leq 1$) or processive ($\alpha > 1$) (Fig S3A). The tracking uncertainty was determined to be 16 nm from the tracked positions of non-motile phagosomes (Fig S3B). Runs were classified as stationary if the run length (R_L) ≤ 16 nm, diffusive if R_L > 16 nm and $\alpha \leq 1$, and processive if R_L > 16 nm and $\alpha > 1$ (Fig. 3A). The MSD for all runs with or without tau, indicates that most EP motility is diffusive (control EPs α = 0.91 and EPs with tau α = 1.0) (Fig 3B). Processive runs had α-values that reflect motor-mediated transport (control EPs α = 1.6 and EPs with tau α = 1.6), whereas runs identified as diffusive had lower α-values (control EPs α = 0.59 and EPs with tau α = 0.61), which indicates that these periods of motility are strictly diffusive (Fig. 3B). Tau

did not change the average lengths of stationary, diffusive, and plus-end directed processive runs but significantly reduced minus-end directed processive runs, whereas the average velocities of all runs remained unchanged (Fig 3C–D). Moreover, tau did not impact the frequency of stationary and diffusive motility but reduced the frequency of processive transport and altered its net directionality (Fig 3E–F). While stationary and diffusive runs were found to be directionally unbiased, 63% of processive transport was directed towards the minus-end in the absence of tau compared to 49% when tau was present (Fig 3F). Combined, these results show that EPs are directionally biased towards the minus-end of microtubules, and tau strongly inhibits minus-end directed motility compared to its effects on plus-end directed motility (Fig 3G).

Tau strongly inhibits long-range minus-end directed processive runs

To dissect tau's role in regulating motor-mediated EP motility, we analyzed the run lengths and velocities of processive runs. Based on the MSD we focused on processive runs with $R_L > 150$ nm (Fig S3A). Further, tau did not have any noticeable effects on the velocities or run length distributions of stationary, diffusive, and processive runs with $R_L < 150$ nm (Figs S4A–C). The distributions of plus-end and minus-end directed processive runs parsed by length closely follow an exponential decay where long runs were rarer than short runs but more frequently directed towards the microtubule minus-end (Fig 4A). Tau reduced the number of long minus-end directed processive runs, while short runs or plus-end directed runs were unaffected (Fig 4A). Minus-end directed processive runs with lower velocities were also less frequent with tau, whereas plus-end directed velocities did not change (Fig 4B). The average run length decreased from 0.49 μm to 0.30 μm and the average velocity increased from 0.25 μm/s to 0.28 μm/s when tau was present, while the average run length and velocities of plus-end processive runs were not significantly affected (Fig. 4C–D). Next, we looked at the relationship between velocity and run length for individual runs. The distribution of control plus-end directed runs followed an approximate linear fit, where velocity increased proportionally to run length (Fig 4E). However, the distribution of minus-end control runs poorly fit a single linear trend and show two distinct populations, where one population consists of runs with faster velocities and shorter run lengths compared to a second population with slower velocities and longer run lengths (Fig 4E). In the presence of tau, the population of slow, long-range minus-end directed runs were more strongly inhibited compared to faster, shorter minus-end runs or plus-end runs (Fig 4E). These findings are surprising as previous single molecule studies showed that tau reduced kinesin-1 run lengths but did not affect dynein run lengths or have any effect on the velocities of either motor (Dixit et al., 2008; Vershinin et al., 2008). These results suggest that for minus-end directed cargoes like EPs, tau acts as an obstacle on the microtubule that more strongly inhibits long dynein-driven runs compared to the relatively short and infrequent kinesin-driven runs.

Tau reduces the forces generated by teams of multiple dynein transporting EPs

To understand how tau regulates the activity of teams of kinesin and dynein, we measured the forces generated by motors transporting EPs along microtubules using an optical trap. Previous studies have shown that isolated LPs exert maximum forces of 9–12 pN *in vitro* and up to ~20 pN in live cells (Rai et al., 2013; Hendricks et al., 2012; Chaudhary et al., 2018; Chaudhary et al., 2019). The maximum forces generated by the sets of motors on isolated EPs reached stall forces of ~8 pN directed towards the microtubule minus-end and ~5 pN directed towards the microtubule plus-end (Fig 5A–B, S5A–B), consistent with fewer motors being associated with EPs than LPs (Fig. 1F–H). EPs rapidly bind to microtubules and exert unidirectional forces directed towards the plus-end or minus-end of microtubules with rare occurrences of phagosomes exerting bidirectional forces (9/63 EPs showed bidirectional forces) (Fig 5A). Consistent with their motility, EPs had a higher fraction of minus-end directed events compared to plus-end directed events (Fig 3F and S5C). A Gaussian Mixture Model was used to identify

sub-populations within the distributions of plus-end and minus-end force events (Fig 5B). Plus-end forces show a peak at 4.3 pN, which is consistent with the stall forces of a single kinesin-1 or kinesin-2 (Schroeder et al., 2012), while the higher fraction of lower forces (~1 pN, 1.9 pN, and 3.2 pN) indicate that kinesins often detach from the microtubule before maximum stall forces are reached (Fig 5B). Low-force events might also be driven by kinesin-3 (Budaitis et al., 2021). Minus-end forces show peaks at multiples of ~1.2 pN (1.4 pN, 2.2 pN, and 3.1 pN), which is consistent with the forces exerted by dynein teams (Rai et al. 2013, Chaudhary et al. 2018). There are also rare minus-end events with higher forces indicated by the peak at ~5.5 pN that includes stall forces up to ~8 pN (Fig 5B). The fraction of minus-end directed force events was reduced in the presence of tau (Fig S5C). Furthermore, tau decreased the frequency of plus-end maximum stall forces shown by the smaller peak at ~4.6 pN, while the frequency of lower force events remained unchanged (Fig 5C–D). However, minus-end directed forces > 5 pN were completely abolished in the presence of tau, followed by a moderate increase in the frequency of lower forces shown by an increase in the magnitude of the peak at ~2.9 pN (Fig 5C–D, S5B). These results indicate that tau decreases the frequency of high force events driven by groups of ~4–8 dynein, with less of an impact on low force events driven by groups of ~1–3 dynein motors.

To compare the effects of tau on the rate at which kinesin and dynein bind to microtubules, we calculated the relative binding rates from the intervals of diffusive dwell times that occurred before each force event in the optical trap (Chaudhary et al., 2019). Tau decreased the relative binding rate of kinesin, whereas the binding rate of dynein increased slightly (Fig 5E). In addition, we compared the effects of tau on the rate at which kinesin and dynein detach from microtubules, by using the method described by Berger et al. (2019), which estimates the force-dependent unbinding rates from the probability that the motors detach within a given range of forces. We found that the unbinding rate for plus-end and minus-end force events with stall durations > 250 msec increased exponentially with force (Fig 5F). However, a higher rate of unbinding also occurred at lower forces (< 1 pN), which indicates that motors transporting EPs frequently unbind from the microtubule independent of force (Fig S5D). Tau increased the unbinding rate of minus-end directed forces, particularly at forces > 3 pN (Fig 5F). In contrast, tau did not affect plus-end forces between 0.5–4.0 pN or significantly alter the unbinding rate (Fig 5E). The lack of an effect of tau on plus-end directed forces is likely due to kinesin-driven forces being rare, consistent with the predominantly minus-end directed motility of EPs (Fig 3). Combined, these results suggest that anterograde EP transport is often driven by a single kinesin engaged at a time and retrograde transport is driven by groups of ~1–3 dynein motors, with rare events driven by ~4–8 dynein motors. In contrast to bidirectional cargoes like LPs, the dynein teams on minus-end directed unidirectional cargoes are more sensitive to tau on microtubules and often detach before maximum forces are exerted.

Discussion

Our results show that tau has disparate effects on the motility of different cargoes. Early phagosomes exhibit fewer long, minus-end directed runs in the presence of tau while tau enhances dynein-directed movement on late phagosomes. Neuronal cytoskeletons are dense and highly complex, which makes it difficult to dissect molecular mechanisms from observations in cells. Therefore, we used *in vitro* reconstitution and single molecule approaches to understand how tau impacts the transport of endogenous cargoes. This system enabled us to measure the motility of phagosomes and use an optical trap to probe for the biophysical effects of tau on their trafficking along microtubules in the absence of other cellular components. Combined, our data supports a model where tau acts as a selective barrier along microtubules

to control the transport of cargoes bound by different sets of motors. We compared early and late phagosomes and found that the types of motors associated with EPs are more variable than LPs, and that EPs associate with fewer dynein and kinesin-2 motors (Fig. 1E-H). The differences in the sets of motors associated with them alters their motility and response to tau (Fig 1B, 2). LPs move bidirectionally (Fig 1B–C), and we showed previously that their plus-end directed forces decreased in the presence of tau, which concomitantly increased the processivity and opposing forces generated by dynein motors along microtubules (Chaudhary et al., 2018). Here, we found that EPs are unidirectional and were more frequently transported towards the minus-end of microtubules (Fig 1B–C, 2A–B). Tau reduced the processivity and maximum forces exerted by teams of dynein on EPs (Fig 4 and 5), which decreased the frequency and travel distances of their minus-end directed transport (Fig 2–4). These findings reveal how tau differentially regulates teams of motors transporting different cargoes (Fig 6). Further, our results suggest that perturbations to tau would be expected to have disparate effects on different types of cargoes.

What determines if a cargo moves unidirectionally or bidirectionally?
Bidirectional motility results from a stochastic tug-of-war between opposing motors that are simultaneously bound to a cargo (Müller et al., 2008). Predictions show that altering the number of kinesin and dynein motors that are bound to a cargo or adjusting their microtubule binding kinetics determines the extent of bidirectional and unidirectional transport (Müller et al., 2008; Soppina et al., 2009; Hendricks et al., 2010; Chaudhary et al., 2018; Ohashi et al., 2019). We reason that EPs exhibit unidirectional motility because they are typically bound by a single type of motor or combinations of two different motors, whereas LPs move bidirectionally because they are simultaneously bound by multiple copies of kinesins-1, -2, -3 and dynein (Fig 1E–F, S2A–B). In support, our optical trapping data shows that EPs exert unidirectional forces that are comparable to the forces produced by a single kinesin or small teams of dynein consisting of ~1–3 motors with rare events driven by teams of ~4–8 motors (Fig 5A–B), whereas the magnitude of the forces exerted by LPs were previously shown to be approximately equal in both directions, which corresponds to forces produced by teams of up to 3 kinesin and 10 dynein motors competing in a tug-of-war along microtubules (Chaudhary et al., 2018). These results further indicate that only a subset of the total number of motors that are bound to cargoes are engaged with microtubules and exert force on EPs. Combined, this data suggests that as phagosomes mature, their total number of motors as well as the ratio of kinesin and dynein motors that engage the microtubule change, which potentiates their transition from unidirectional to bidirectional transport.

While our data show that early and late phagosomes exhibit different motility due to being associated with different sets of kinesin and dynein motors, other factors likely modulate the activity of vesicle-bound motors. In *Dictyostelium,* phagosomes examined at 5–10 and 30 minutes following bead uptake, were shown to transition from bidirectional to unidirectional retrograde transport (Rai et al., 2016). As phagosomes mature, multiple dynein motors cluster within cholesterol-rich microdomains along their surface, which enables them to collectively exert higher forces (Rai et al., 2016). Thus, clusters of dynein can more effectively outcompete single diffuse kinesins, which promotes the transition from bidirectional to unidirectional retrograde transport. Furthermore, transport may also be differentially controlled in specific regions of the cell by transient motor-cargo interactions. For example, the directionality of early endosomes in filamentous fungi is governed by the transient binding of dynein that outcompetes kinesin-3 motors causing them to switch between plus-end and minus-end directed transport as they approach the hyphal tip, where pools of dynein are most concentrated (Schuster et al., 2011). Similar mechanisms could ensure that phagosome trafficking is spatially and temporally

controlled as they mature, where different motors transiently interact with EPs and LPs or are reorganized on their membranes to bias their trafficking in different regions of the cell.

Adaptor proteins are functionally diverse and associate with different motors to control cargo motility. Adaptor-motor complexes have been shown to recognize different cargoes through direct or indirect interactions with Rab GTPases and other membrane associated regulatory effectors (Cantalupo et al., 2001; Jordens et al., 2001; Niwa et al., 2008; Schonteich et al., 2008; Arimura et al., 2009; Horgan et al., 2010; Ueno et al., 2011; Christensen et al., 2021). As phagosomes mature, the level of Rabs and other small GTPases change (Goyette et al., 2009). Therefore, it is possible that these changes generate downstream effects that alter the type of adaptors and motors that associate with early and late phagosomes, which in turn impact their motility. Adaptor proteins orchestrate bidirectional motility or enhance transport by scaffolding multiple kinesin and dynein motors (Akhmanova and Hammer et al., 2010; Fu and Holzbaur, 2013; Bielska et al., 2014; Kendrick et al., 2019; Fenton et al., 2021). Adaptors also modulate the effect of tau on motor motility. TRAK1, which is a mitochondrial specific adaptor protein, is an example of an adaptor that enhances anterograde transport, where it activates and tethers kinesin-1 to the microtubule surface enabling it to robustly transport mitochondria over long distances and through dense tau patches along microtubules (Henrichs et al., 2020). While several adaptors have been identified to control the motility of different organelles and vesicular cargoes, those that associate with phagosomes are not fully characterized. Yet, different adaptor-motor complexes likely associate with EPs and LPs, and contribute to differences in their motility and responses to tau by regulating both the recruitment and activity of phagosome-bound motors.

How are cargoes with different sets of motors selectively regulated along tau-decorated microtubules?

Our work illustrates that the response of organelle motility to tau is not fully predicted from the response of single motor proteins to tau. Previous studies investigated tau's impact on the motility of single motors or groups of homogenous motors and showed that kinesin-1 and kinesin-3 are more strongly inhibited by tau than kinesin-2 and dynein (Vershinin et al., 2007; Dixit et al., 2008; Vershinin et al., 2008; McVicker et al., 2011; Hoeprich et al., 2014; Hoeprich et al., 2017; Monroy et al., 2018; Tan et al., 2019). It is becoming more clear that tau acts like a roadblock for certain motors depending on their structure as well as their microtubule binding kinetics. Kinesin-1 predominantly moves by stepping forward toward the plus-end of microtubules along a single protofilament, while dynein moves with less precision but is capable of side-stepping to adjacent protofilaments and even reversing directions (DeWitt et al., 2012). Kinesin-2 is also capable of side-stepping due to its more flexible neck linker (Shastry and Hancock, 2010; Hoeprich et al., 2014; Hoeprich et al., 2017). Because of their less restrained movement, it is thought that kinesin-2 and dynein are better at navigating around tau patches compared to kinesin-1 and kinesin-3 that move more rigidly along microtubules. Thus, single-molecule studies would predict that dynein-driven transport would be insensitive to tau, while we observe that the long-range transport of EPs mediated by dynein is strongly inhibited by tau.

Emerging evidence also suggests that motor detachment and reattachment kinetics play a pivotal role during transport and could influence how cargoes respond to MAPs. Kinesin-1 provides more sustained force during transport but reattaches slowly after it detaches from the microtubule, whereas kinesin-2 and kinesin-3 frequently detach from microtubules under load but reattach much faster than kinesin-1 (Feng et al., 2018; Arpağ et al., 2019). Because their binding rates are much faster than their unbinding rates, kinesin-2 and kinesin-3 can more efficiently probe for available landing sites along microtubules, which helps tether the cargo close to the microtubule and navigate around obstacles. These studies could explain how

cooperation between motors, for instance those that produce force and others that may act as a tether, enable cargoes to endure long distance travel over several microns (Fig 2A–B). Although EPs travel further distances, because they are bound by fewer types of motors, they may be more prone to inhibition by tau compared to cargoes that are bound by multiple types of motors like LPs, in which more kinesin and dynein motors engage the microtubule simultaneously to bypass tau (Chaudhary et al., 2018).

In neurons, several mechanisms must coordinate to ensure that cargoes are delivered with precision over long distances. MAPs that differentially impact the motility of kinesin and dynein motors compete for space along microtubules to govern the transport of intracellular cargoes (Monroy et al., 2018; Chaudhary et al., 2019; Monroy et al., 2020). Microtubules within the axon that are decorated by tau could modulate directional transport or function as selective tracks for certain cargoes, whereas microtubules that are bound by different MAPs act as selective tracks for other types of cargoes. Our results suggest that tau functions as a barrier along microtubules to selectively inhibit some cargoes while allowing the passage of others depending on the type of motors and adaptors driving their transport. Tau is also regulated by post-translational modifications and isoform expression, which could influence its affinity for microtubules as well as its impact on the motility of different motors. Our studies indicate that regulating tau dynamics through post-translational modifications or disease mutations would be expected to have cargo-specific effects on transport.

Materials and methods

Cell culture and live cell imaging

J774A.1 mouse macrophage (ATCC) were maintained in DMEM (Gibco), supplemented with 10% fetal bovine serum (Thermo Fisher Scientific) and 1% GlutaMAX (Gibco) at 37°C with 5% CO_2.
Macrophages were treated with BSA-coated 200nm fluorescent beads and imaged using TIRF microscopy (*SI Appendix*, *Methods*) 30–45 mins after bead uptake to visualize bead-containing early phagosomes and 90 mins after uptake to visualize late phagosomes (LPs). The mode of transport, directionality, displacement, and number of reversals for all phagosome trajectories were analyzed using custom MATLAB scripts developed in our lab.

Immunofluorescence imaging

Isolated early and late phagosomes (*SI Appendix*, *Methods*) were added to silanized coverslips mounted to microscope slides using vacuum grease and double-sided tape to make flow chambers (Dixit and Ross, 2010) and incubated for 1 hour at room temperature (RT) to allow them to adhere to the surface. Following the incubation, chambers were washed 2X with MAB before and after treatment with Pluronic F-127 to prevent non-specific binding before incubation with primary antibodies. Phagosomes were incubated with different combinations of primary antibodies for kinesin-1 (MAB1614, EMD Millipore), kinesin-2 (ab24626, Abcam) conjugated to Alexa568 (A20184, Thermo Fisher Scientific), dynein (sc-9115, Santa Cruz), kif16b (SAB1401759, Sigma), and kif1b (MABC309, EMD Millipore) for 1 hour at RT in the dark. Following treatment with primary antibodies, phagosomes were washed 3X with MAB and incubated with secondary antibodies against mouse (Alexa488; A11029, Thermo Fisher Scientific) and rabbit (Alexa647; A32733, Thermo Fisher Scientific) for 1 hour at RT in the dark. Samples were washed 3X with MAB before imaging. Multichannel images were acquired in brightfield or with 500 msec exposures in TIRF using the 488 nm, 561 nm, and 640 nm lasers, set between 1–5% power. Thresholds > 800 a.u. were applied to compare the type of motors on EPs and LPs. Only phagosomes with fluorescence signals above the threshold were counted.

Stepwise photobleaching analysis

Phagosomes (*SI Appendix*, *Methods*) were incubated in flow chambers for 1 hour and treated with Pluronic F-127 as described above. Separate chambers were used for each motor counted. Phagosomes in each chamber were incubated with one of the following mouse monoclonal antibodies against kinesin-1 (MAB1614, EMD Millipore), kinesin-2 (ab24626, Abcam), kif16b (SAB1401759, Sigma), kif1b (MABC309, EMD Millipore), and dynein (MAB1618, EMD Millipore) for 2 hours at RT in the dark. Chambers were washed 3X with MAB and incubated with anti-mouse Alexa647 (A21236, Thermo Fisher Scientific) secondary antibody for 1.5 hours. Following, chambers were washed 3X with MAB. Phagosomes were imaged in epifluorescence with 500 msec exposures using a 640 nm laser at 3 mW. Recombinant rat kinesin-1 (rkin430-GFP; A gift from Dr. Gary Brouhard, Dept. Biology, McGill University) was imaged under similar conditions to determine the number of steps for a single motor. Purified kinesin-1 was diluted to 10 nM and incubated with primary and secondary antibodies and bound to unlabeled microtubules using 1 mM AMPNP to detect single statically bound molecules. Images were acquired similar to phagosomes but instead using TIRF to achieve detectable steps. Only steps > 15 a.u. were considered. For kinesin-2, the number of steps was multiplied by a factor of 2 since it exists as a heterodimer and contains 1 epitope recognized by the antibody. A step-finding algorithm (Chen et al., 2014) was used to determine the number and size of photobleaching steps for single motors and for the sets of motors on phagosomes. The mean step size was determined to be 21 a.u. for kinesins -1 and -2 and dynein, 30 a.u. for kif16b and kif1b, and 52 a.u. for recombinant single molecule kinesin-1. The number of steps was determined by dividing the difference between the initial and final fluorescence intensity by the mean step size.

***In vitro* motility assays**

Flow chambers were first incubated with anti-β-tubulin (T4026 clone TUB2.1, Sigma) diluted 2:50 in BRB80 for 5 mins. Chambers were then treated with F-127 for 5 mins and washed 2X with T-BRB80. Polarity marked microtubules (*SI Appendix*, *Methods*) were added to the chambers and incubated for 5 mins at RT. Unbound microtubules were washed out with 2X T-BRB80. Isolated phagosomes (*SI Appendix*, *Methods*) were flown through the chamber supplemented with 0.2 mg/ml BSA, 10 mM DTT, 1 mM MgATP, 20 μM Taxol, 15 mg/ml glucose, ≥ 2000 units/g glucose oxidase, ≥ 6 units/g catalase, and 1 mg/ml casein. For experiments with tau, microtubules were incubated with 10 nM of Alexa568 labeled 3RS-tau for 30 mins. Tau protein was expressed and purified as previously described in Chaudhary et al., (2018). Phagosome mixtures were also supplemented with 10 nM tau. Using TIRF, microtubules and tau were imaged for 1 frame with the 561 nm and 640 nm lasers at 1–10% power and time lapse recordings of phagosomes were imaged with 80 msec exposures using a 450 nm laser set at 2% power for 5 mins.

Optical trapping

Optical trapping was performed similar to motility assays, except using a 10 W, 1064 nm laser (IPG Photonics) to trap phagosomes, a quadrant photodiode detector (QPD) (PDP90A, Thorlabs) to sense the displacement and forces exerted by phagosomes away from the trap center, and TIRF microscopy to position phagosomes over microtubules. The trap stiffness and positional calibration was determined by fitting a Lorentzian function to the power spectrum of thermal fluctuations of trapped phagosomes. Forces were calculated by measuring the displacement of the trapped phagosome from the trap center, where the displacement is directly proportional to the trap stiffness. Forces were filtered by stall time and analyzed using custom MATLAB codes to measure the magnitudes, frequency of events, and the relative binding and unbinding rates.

Statistical analysis

All data were presented with error bars indicating standard error of the mean (SEM) or 95% confidence intervals when specified in the figure legends. All *n* and number of replicates were mentioned in the figure legends. Bootstrapping analysis was performed in MATLAB and used to test for statistical significance and determine confidence intervals. Kolmogrov-Smirnov test was used to test for statistical significance of tau's effect on the distribution of run lengths, velocities, force events, and relative binding rates.

Acknowledgements

The authors thank Dr. Gary Brouhard for providing reagents and Dr. Florian Berger for providing assistance with unbinding data analysis. We thank Mahmoud Nour for providing assistance with the change point analysis. This work was supported by NIH.

Author Contributions: DB and AGH conceptualized and designed this work. DB performed experiments and analysis. DB and AGH wrote the manuscript and made the figures, CLB contributed reagents, CLB and AGH obtained funding for this work.

References

Akhmanova A, Hammer JA 3rd. Linking molecular motors to membrane cargo. Curr Opin Cell Biol. 2010 Aug;22(4):479-87.

Arimura N, Kimura T, Nakamuta S, Taya S, Funahashi Y, Hattori A, Shimada A, Ménager C, Kawabata S, Fujii K, Iwamatsu A, Segal RA, Fukuda M, Kaibuchi K. Anterograde transport of TrkB in axons is mediated by direct interaction with Slp1 and Rab27. Dev Cell. 2009 May;16(5):675-86.

Arpağ G, Norris SR, Mousavi SI, Soppina V, Verhey KJ, Hancock WO, Tüzel E. Motor Dynamics Underlying Cargo Transport by Pairs of Kinesin-1 and Kinesin-3 Motors. Biophys J. 2019 Mar 19;116(6):1115-1126.

Balabanian L, Berger CL, Hendricks AG. Acetylated Microtubules Are Preferentially Bundled Leading to Enhanced Kinesin-1 Motility. Biophys J. 2017 Oct 3;113(7):1551-1560.

Bentley M, Decker H, Luisi J, Banker G. A novel assay reveals preferential binding between Rabs, kinesins, and specific endosomal subpopulations. J Cell Biol. 2015 Feb 2;208(3):273-81.

Berger F, Klumpp S, Lipowsky R. Force-Dependent Unbinding Rate of Molecular Motors from Stationary Optical Trap Data. Nano Lett. 2019 Apr 10;19(4):2598-2602.

Bielska E, Schuster M, Roger Y, Berepiki A, Soanes DM, Talbot NJ, Steinberg G. Hook is an adapter that coordinates kinesin-3 and dynein cargo attachment on early endosomes. J Cell Biol. 2014 Mar 17;204(6):989-1007.

Blatner NR, Wilson MI, Lei C, Hong W, Murray D, Williams RL, Cho W. The structural basis of novel endosome anchoring activity of KIF16B kinesin. EMBO J. 2007 Aug 8;26(15):3709-19.

Blocker A, Severin FF, Burkhardt JK, Bingham JB, Yu H, Olivo JC, Schroer TA, Hyman AA, Griffiths G. Molecular requirements for bi-directional movement of phagosomes along microtubules. J Cell Biol. 1997 Apr 7;137(1):113-29.

Brown CL, Maier KC, Stauber T, Ginkel LM, Wordeman L, Vernos I, Schroer TA. Kinesin-2 is a motor for late endosomes and lysosomes. Traffic. 2005 Dec;6(12):1114-24.

Budaitis BG, Jariwala S, Rao L, Yue Y, Sept D, Verhey KJ, Gennerich A. Pathogenic mutations in the kinesin-3 motor KIF1A diminish force generation and movement through allosteric mechanisms. J Cell Biol. 2021 Apr 5;220(4):e202004227.

Cantalupo G, Alifano P, Roberti V, Bruni CB, Bucci C. Rab-interacting lysosomal protein (RILP): the Rab7 effector required for transport to lysosomes. EMBO J. 2001 Feb 15;20(4):683-93.

Chaudhary AR, Berger F, Berger CL, Hendricks AG. Tau directs intracellular trafficking by regulating the forces exerted by kinesin and dynein teams. Traffic. 2018 Feb;19(2):111-121.

Chaudhary AR, Lu H, Krementsova EB, Bookwalter CS, Trybus KM, Hendricks AG. MAP7 regulates organelle transport by recruiting kinesin-1 to microtubules. J Biol Chem. 2019 Jun 28;294(26):10160-10171.

Chen Y, Deffenbaugh NC, Anderson CT, Hancock WO. Molecular counting by photobleaching in protein complexes with many subunits: best practices and application to the cellulose synthesis complex. Mol Biol Cell. 2014 Nov 5;25(22):3630-42.

Christensen JR, Kendrick AA, Truong JB, Aguilar-Maldonado A, Adani V, Dzieciatkowska M, Reck-Peterson SL. Cytoplasmic dynein-1 cargo diversity is mediated by the combinatorial assembly of FTS-Hook-FHIP complexes. Elife. 2021 Dec 9;10:e74538.

Desjardins M, Huber LA, Parton RG, Griffiths G. Biogenesis of phagolysosomes proceeds through a sequential series of interactions with the endocytic apparatus. J Cell Biol. 1994 Mar;124(5):677-88.

Desjardins M, Celis JE, van Meer G, Dieplinger H, Jahraus A, Griffiths G, Huber LA. Molecular characterization of phagosomes. J Biol Chem. 1994 Dec 23;269(51):32194-200.

DeWitt MA, Chang AY, Combs PA, Yildiz A. Cytoplasmic dynein moves through uncoordinated stepping of the AAA+ ring domains. Science. 2012 Jan 13;335(6065):221-5.

Dixit R, Ross JL, Goldman YE, Holzbaur EL. Differential regulation of dynein and kinesin motor proteins by tau. Science. 2008 Feb 22;319(5866):1086-9.

Dixit R, Ross JL. Studying plus-end tracking at single molecule resolution using TIRF microscopy. Methods Cell Biol. 2010;95:543-54.

Feng Q, Mickolajczyk KJ, Chen GY, Hancock WO. Motor Reattachment Kinetics Play a Dominant Role in Multimotor-Driven Cargo Transport. Biophys J. 2018 Jan 23;114(2):400-409.

Fenton AR, Jongens TA, Holzbaur ELF. Mitochondrial adaptor TRAK2 activates and functionally links opposing kinesin and dynein motors. Nat Commun. 2021 Jul 28;12(1):4578.

Ferro LS, Fang Q, Eshun-Wilson L, Fernandes J, Jack A, Farrell DP, Golcuk M, Huijben T, Costa K, Gur M, DiMaio F, Nogales E, Yildiz A. Structural and functional insight into regulation of kinesin-1 by microtubule-associated protein MAP7. Science. 2022 Jan 21;375(6578):326-331.

Flores-Rodriguez N, Rogers SS, Kenwright DA, Waigh TA, Woodman PG, Allan VJ. Roles of dynein and dynactin in early endosome dynamics revealed using automated tracking and global analysis. PLoS One. 2011;6(9):e24479.

Fu MM, Holzbaur EL. JIP1 regulates the directionality of APP axonal transport by coordinating kinesin and dynein motors. J Cell Biol. 2013 Aug 5;202(3):495-508.

Garin J, Diez R, Kieffer S, Dermine JF, Duclos S, Gagnon E, Sadoul R, Rondeau C, Desjardins M. The phagosome proteome: insight into phagosome functions. J Cell Biol. 2001 Jan 8;152(1):165-80.

Goyette G, Boulais J, Carruthers NJ, Landry CR, Jutras I, Duclos S, Dermine JF, Michnick SW, LaBoissière S, Lajoie G, Barreiro L, Thibault P, Desjardins M. Proteomic characterization of phagosomal membrane microdomains during phagolysosome biogenesis and evolution. Mol Cell Proteomics. 2012 Nov;11(11):1365-77.

Gross SP, Welte MA, Block SM, Wieschaus EF. Coordination of opposite-polarity microtubule motors. J Cell Biol. 2002 Feb 18;156(4):715-24.

Guardia CM, Farías GG, Jia R, Pu J, Bonifacino JS. BORC Functions Upstream of Kinesins 1 and 3 to Coordinate Regional Movement of Lysosomes along Different Microtubule Tracks. Cell Rep. 2016 Nov 15;17(8):1950-1961.

Gumy LF, Katrukha EA, Grigoriev I, Jaarsma D, Kapitein LC, Akhmanova A, Hoogenraad CC. MAP2 Defines a Pre-axonal Filtering Zone to Regulate KIF1- versus KIF5-Dependent Cargo Transport in Sensory Neurons. Neuron. 2017 Apr 19;94(2):347-362.e7.

Gyparaki MT, Arab A, Sorokina EM, Santiago-Ruiz AN, Bohrer CH, Xiao J, Lakadamyali M. Tau forms oligomeric complexes on microtubules that are distinct from tau aggregates. Proc Natl Acad Sci U S A. 2021 May 11;118(19):e2021461118.

Harterink M, Edwards SL, de Haan B, Yau KW, van den Heuvel S, Kapitein LC, Miller KG, Hoogenraad CC. Local microtubule organization promotes cargo transport in C. elegans dendrites. J Cell Sci. 2018 Oct 22;131(20):jcs223107.

Hendricks AG, Perlson E, Ross JL, Schroeder HW 3rd, Tokito M, Holzbaur EL. Motor coordination via a tug-of-war mechanism drives bidirectional vesicle transport. Curr Biol. 2010 Apr 27;20(8):697-702.

Hendricks AG, Holzbaur EL, Goldman YE. Force measurements on cargoes in living cells reveal collective dynamics of microtubule motors. Proc Natl Acad Sci U S A. 2012 Nov 6;109(45):18447-52.

Henrichs V, Grycova L, Barinka C, Nahacka Z, Neuzil J, Diez S, Rohlena J, Braun M, Lansky Z. Mitochondria-adaptor TRAK1 promotes kinesin-1 driven transport in crowded environments. Nat Commun. 2020 Jun 19;11(1):3123.

Hinrichs MH, Jalal A, Brenner B, Mandelkow E, Kumar S, Scholz T. Tau protein diffuses along the microtubule lattice. J Biol Chem. 2012 Nov 9;287(46):38559-68.

Hirokawa N, Noda Y, Tanaka Y, Niwa S. Kinesin superfamily motor proteins and intracellular transport. Nat Rev Mol Cell Biol. 2009 Oct;10(10):682-96.

Hoepfner S, Severin F, Cabezas A, Habermann B, Runge A, Gillooly D, Stenmark H, Zerial M. Modulation of receptor recycling and degradation by the endosomal kinesin KIF16B. Cell. 2005 May 6;121(3):437-50.

Hoeprich GJ, Thompson AR, McVicker DP, Hancock WO, Berger CL. Kinesin's neck-linker determines its ability to navigate obstacles on the microtubule surface. Biophys J. 2014 Apr 15;106(8):1691-700.

Hoeprich GJ, Mickolajczyk KJ, Nelson SR, Hancock WO, Berger CL. The axonal transport motor kinesin-2 navigates microtubule obstacles via protofilament switching. Traffic. 2017 May;18(5):304-314.

Hooikaas PJ, Martin M, Mühlethaler T, Kuijntjes GJ, Peeters CAE, Katrukha EA, Ferrari L, Stucchi R, Verhagen DGF, van Riel WE, Grigoriev I, Altelaar AFM, Hoogenraad CC, Rüdiger

SGD, Steinmetz MO, Kapitein LC, Akhmanova A. MAP7 family proteins regulate kinesin-1 recruitment and activation. J Cell Biol. 2019 Apr 1;218(4):1298-1318.

Horgan CP, Hanscom SR, Jolly RS, Futter CE, McCaffrey MW. Rab11-FIP3 links the Rab11 GTPase and cytoplasmic dynein to mediate transport to the endosomal-recycling compartment. J Cell Sci. 2010 Jan 15;123(Pt 2):181-91.

Hummel JJA, Hoogenraad CC. Inducible manipulation of motor-cargo interaction using engineered kinesin motors. J Cell Sci. 2021 Aug 1;134(15):jcs258776.

Jenkins B, Decker H, Bentley M, Luisi J, Banker G. A novel split kinesin assay identifies motor proteins that interact with distinct vesicle populations. J Cell Biol. 2012 Aug 20;198(4):749-61.

Jordens I, Fernandez-Borja M, Marsman M, Dusseljee S, Janssen L, Calafat J, Janssen H, Wubbolts R, Neefjes J. The Rab7 effector protein RILP controls lysosomal transport by inducing the recruitment of dynein-dynactin motors. Curr Biol. 2001 Oct 30;11(21):1680-5.

Kellogg EH, Howes S, Ti SC, Ramírez-Aportela E, Kapoor TM, Chacón P, Nogales E. Near-atomic cryo-EM structure of PRC1 bound to the microtubule. Proc Natl Acad Sci U S A. 2016 Aug 23;113(34):9430-9.

Kendrick AA, Dickey AM, Redwine WB, Tran PT, Vaites LP, Dzieciatkowska M, Harper JW, Reck-Peterson SL. Hook3 is a scaffold for the opposite-polarity microtubule-based motors cytoplasmic dynein-1 and KIF1C. J Cell Biol. 2019 Sep 2;218(9):2982-3001.

Lipka J, Kapitein LC, Jaworski J, Hoogenraad CC. Microtubule-binding protein doublecortin-like kinase 1 (DCLK1) guides kinesin-3-mediated cargo transport to dendrites. EMBO J. 2016 Feb 1;35(3):302-18.

Liu JS, Schubert CR, Fu X, Fourniol FJ, Jaiswal JK, Houdusse A, Stultz CM, Moores CA, Walsh CA. Molecular basis for specific regulation of neuronal kinesin-3 motors by doublecortin family proteins. Mol Cell. 2012 Sep 14;47(5):707-21.

Loubéry S, Wilhelm C, Hurbain I, Neveu S, Louvard D, Coudrier E. Different microtubule motors move early and late endocytic compartments. Traffic. 2008 Apr;9(4):492-509.

Mandelkow EM, Stamer K, Vogel R, Thies E, Mandelkow E. Clogging of axons by tau, inhibition of axonal traffic and starvation of synapses. Neurobiol Aging. 2003 Dec;24(8):1079-85.

Matsushita M, Tanaka S, Nakamura N, Inoue H, Kanazawa H. A novel kinesin-like protein, KIF1Bbeta3 is involved in the movement of lysosomes to the cell periphery in non-neuronal cells. Traffic. 2004 Mar;5(3):140-51.

McVicker DP, Chrin LR, Berger CL. The nucleotide-binding state of microtubules modulates kinesin processivity and the ability of Tau to inhibit kinesin-mediated transport. J Biol Chem. 2011 Dec 16;286(50):42873-80.

McVicker DP, Hoeprich GJ, Thompson AR, Berger CL. Tau interconverts between diffusive and stable populations on the microtubule surface in an isoform and lattice specific manner. Cytoskeleton (Hoboken). 2014 Mar;71(3):184-94.

Monroy BY, Sawyer DL, Ackermann BE, Borden MM, Tan TC, Ori-McKenney KM. Competition between microtubule-associated proteins directs motor transport. Nat Commun. 2018 Apr 16;9(1):1487.

Monroy BY, Tan TC, Oclaman JM, Han JS, Simó S, Niwa S, Nowakowski DW, McKenney RJ, Ori-McKenney KM. A Combinatorial MAP Code Dictates Polarized Microtubule Transport. Dev Cell. 2020 Apr 6;53(1):60-72.e4.

Müller MJ, Klumpp S, Lipowsky R. Tug-of-war as a cooperative mechanism for bidirectional cargo transport by molecular motors. Proc Natl Acad Sci U S A. 2008 Mar 25;105(12):4609-14.

Niwa S, Tanaka Y, Hirokawa N. KIF1Bbeta- and KIF1A-mediated axonal transport of presynaptic regulator Rab3 occurs in a GTP-dependent manner through DENN/MADD. Nat Cell Biol. 2008 Nov;10(11):1269-79.

Ohashi KG, Han L, Mentley B, Wang J, Fricks J, Hancock WO. Load-dependent detachment kinetics plays a key role in bidirectional cargo transport by kinesin and dynein. Traffic. 2019 Apr;20(4):284-294.

Pu J, Guardia CM, Keren-Kaplan T, Bonifacino JS. Mechanisms and functions of lysosome positioning. J Cell Sci. 2016 Dec 1;129(23):4329-4339.

Rai AK, Rai A, Ramaiya AJ, Jha R, Mallik R. Molecular adaptations allow dynein to generate large collective forces inside cells. Cell. 2013 Jan 17;152(1-2):172-82.

Rai A, Pathak D, Thakur S, Singh S, Dubey AK, Mallik R. Dynein Clusters into Lipid Microdomains on Phagosomes to Drive Rapid Transport toward Lysosomes. Cell. 2016 Feb 11;164(4):722-34.

Reck-Peterson SL, Redwine WB, Vale RD, Carter AP. The cytoplasmic dynein transport machinery and its many cargoes. Nat Rev Mol Cell Biol. 2018 Jun;19(6):382-398.

Rosa-Ferreira C, Munro S. Arl8 and SKIP act together to link lysosomes to kinesin-1. Dev Cell. 2011 Dec 13;21(6):1171-8.

Ruhnow F, Zwicker D, Diez S. Tracking single particles and elongated filaments with nanometer precision. Biophys J. 2011 Jun 8;100(11):2820-8.

Schonteich E, Wilson GM, Burden J, Hopkins CR, Anderson K, Goldenring JR, Prekeris R. The Rip11/Rab11-FIP5 and kinesin II complex regulates endocytic protein recycling. J Cell Sci. 2008 Nov 15;121(Pt 22):3824-33.

Schroeder HW 3rd, Hendricks AG, Ikeda K, Shuman H, Rodionov V, Ikebe M, Goldman YE, Holzbaur EL. Force-dependent detachment of kinesin-2 biases track switching at cytoskeletal filament intersections. Biophys J. 2012 Jul 3;103(1):48-58.

Schuster M, Lipowsky R, Assmann MA, Lenz P, Steinberg G. Transient binding of dynein controls bidirectional long-range motility of early endosomes. Proc Natl Acad Sci U S A. 2011 Mar 1;108(9):3618-23.

Siahaan V, Krattenmacher J, Hyman AA, Diez S, Hernández-Vega A, Lansky Z, Braun M. Kinetically distinct phases of tau on microtubules regulate kinesin motors and severing enzymes. Nat Cell Biol. 2019 Sep;21(9):1086-1092.

Shastry S, Hancock WO. Neck linker length determines the degree of processivity in kinesin-1 and kinesin-2 motors. Curr Biol. 2010 May 25;20(10):939-43.

Soppina V, Rai AK, Ramaiya AJ, Barak P, Mallik R. Tug-of-war between dissimilar teams of microtubule motors regulates transport and fission of endosomes. Proc Natl Acad Sci U S A. 2009 Nov 17;106(46):19381-6.

Tan R, Lam AJ, Tan T, Han J, Nowakowski DW, Vershinin M, Simó S, Ori-McKenney KM, McKenney RJ. Microtubules gate tau condensation to spatially regulate microtubule functions. Nat Cell Biol. 2019 Sep;21(9):1078-1085.

Tinevez JY, Perry N, Schindelin J, Hoopes GM, Reynolds GD, Laplantine E, Bednarek SY, Shorte SL, Eliceiri KW. TrackMate: An open and extensible platform for single-particle tracking. Methods. 2017 Feb 15;115:80-90.

Ueno H, Huang X, Tanaka Y, Hirokawa N. KIF16B/Rab14 molecular motor complex is critical for early embryonic development by transporting FGF receptor. Dev Cell. 2011 Jan 18;20(1):60-71.

Vershinin M, Carter BC, Razafsky DS, King SJ, Gross SP. Multiple-motor based transport and its regulation by Tau. Proc Natl Acad Sci U S A. 2007 Jan 2;104(1):87-92.

Vershinin M, Xu J, Razafsky DS, King SJ, Gross SP. Tuning microtubule-based transport through filamentous MAPs: the problem of dynein. Traffic. 2008 Jun;9(6):882-92.

Welte MA. Bidirectional transport along microtubules. Curr Biol. 2004 Jul 13;14(13):R525-37.

Cella Zanacchi F, Manzo C, Magrassi R, Derr ND, Lakadamyali M. Quantifying Protein Copy Number in Super Resolution Using an Imaging-Invariant Calibration. Biophys J. 2019 Jun 4;116(11):2195-2203.

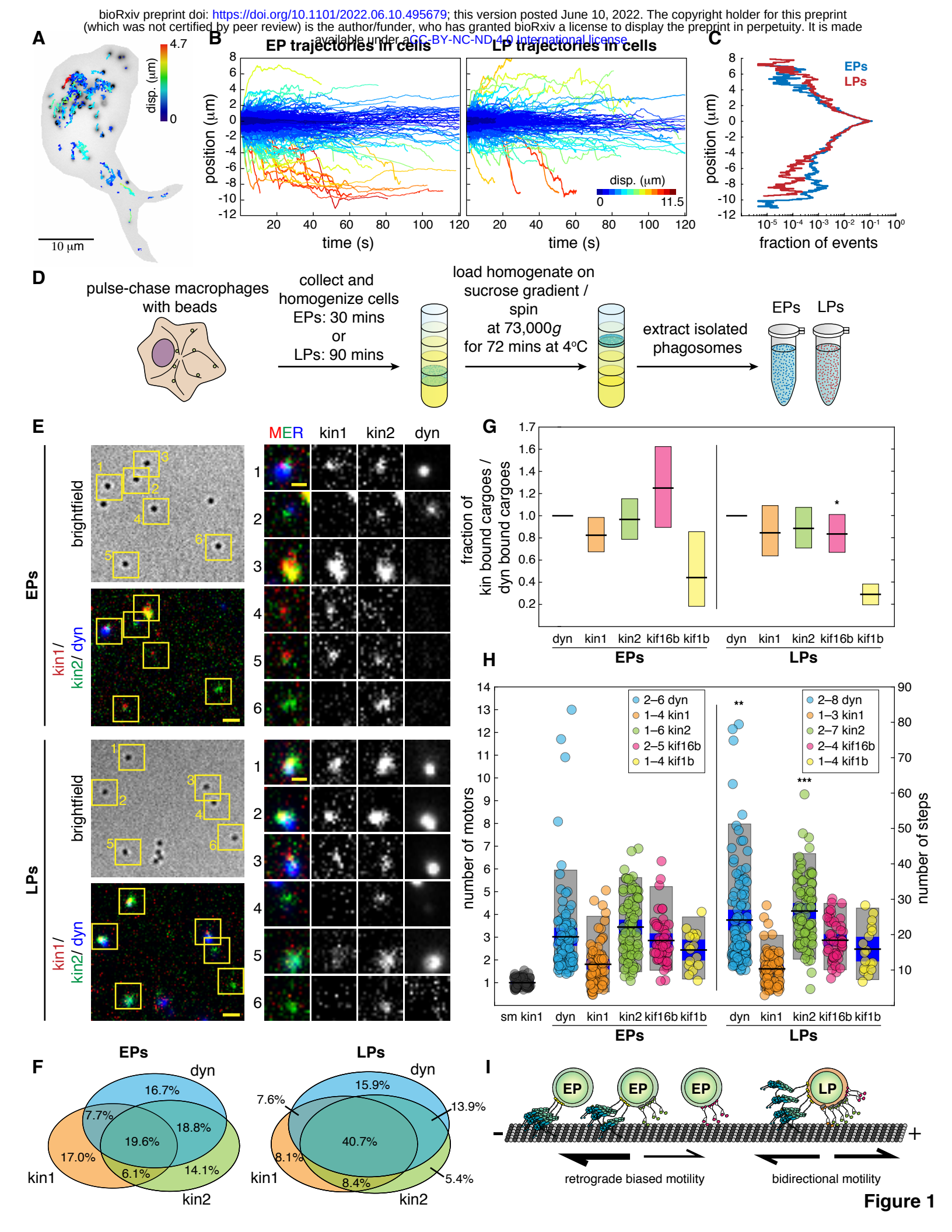

Figure 1

Figure 1) EPs and LPs exhibit diverse motility and are transported by different sets of motors

A) An image shows a J774A.1 mouse macrophage treated with 200 nm latex fluorescent beads. The image is overlayed with positional tracking data obtained from TrackMate and color coded by displacement. Time-lapse images were acquired 30–45 mins or > 90 mins after bead uptake to visualize bead-containing early phagosomes (EPs) or late phagosomes (LPs), respectively. Scale bar is 10 μm. **B)** The plots show the displacement of EPs (2211 trajectories from 9 cells) and LPs (1579 trajectories from 7 cells) towards the cell center (minus-end direction) or the cell periphery (plus-end direction). **C)** A plot shows the fraction of plus-end and minus-end EP and LP trajectories as a function of displacement. **D)** A cartoon schematic of the steps to isolate phagosomes from cells. EPs were collected at 30 mins and LPs were collected at 90 mins after bead uptake. **E)** Images show isolated EPs (top panel) and LPs (bottom panel) immunostained for kinesin-1 (red), kinesin-2 (green), and dynein (blue). On the right, zoomed in ROIs show examples of the different combinations of motors on individual phagosomes. Scale bars are 2 μm or 1 μm for selected ROIs. **F)** Venn diagrams show the mean percentages of individual motors and combinations of motors on EPs (n = 230) and LPs (n = 239). **G)** A plot shows the fraction of phagosomes that were positive for kinesins-1, -2, kif16b and kif1b compared to the number of phagosomes that were positive for dynein. Black lines indicate mean values and boxes show 90% confidence intervals generated by bootstrapping analysis with replacement for the number of positive phagosomes for each field of view (* $p < 0.05$). **H)** Stepwise photobleaching analysis was used to estimate the number of motors that associate with EPs and LPs. A plot shows the distributions of the number of kinesin-1, kinesin-2, kif16b, kif1b, and dynein motors on EPs and LPs, mean values (black lines), SEM (blue bars), and 90% confidence intervals (light grey bars). Single molecule kinesin-1 (sm kin1) was used to estimate the number of steps for a single motor (n = 59). The step counts indicate that there were 1–4 kinesin-1 on EPs (n = 79) and 1–3 kinesin-1 on LPs (n = 82), 1–6 kinesin-2 on EPs (n = 82) and 1–7 kinesin-2 on LPs (n = 83), 2–5 kif16b on EPs (n = 51) and 2–4 kif16b on LPs (n = 49), 1–4 kif1b on both EPs (n = 16) and LPs (n = 17), and 2–6 dynein on EPs (n = 101) and 2–8 dynein on LPs (n = 107). Bootstrapping analysis of the mean steps of each motor on EPs compared to LPs was performed to test for statistical significance (** $p < 0.01$, *** $p < 0.0001$). **I)** The schematic depicts the correlation between the sets of motors and the motility of cargoes. EPs are more diverse and often bound by one type of a motor or a combination of two different motors and exhibit biased unidirectional minus-end transport, whereas LPs are more homogenous and bound by groups of opposing motors and exhibit bidirectional transport.

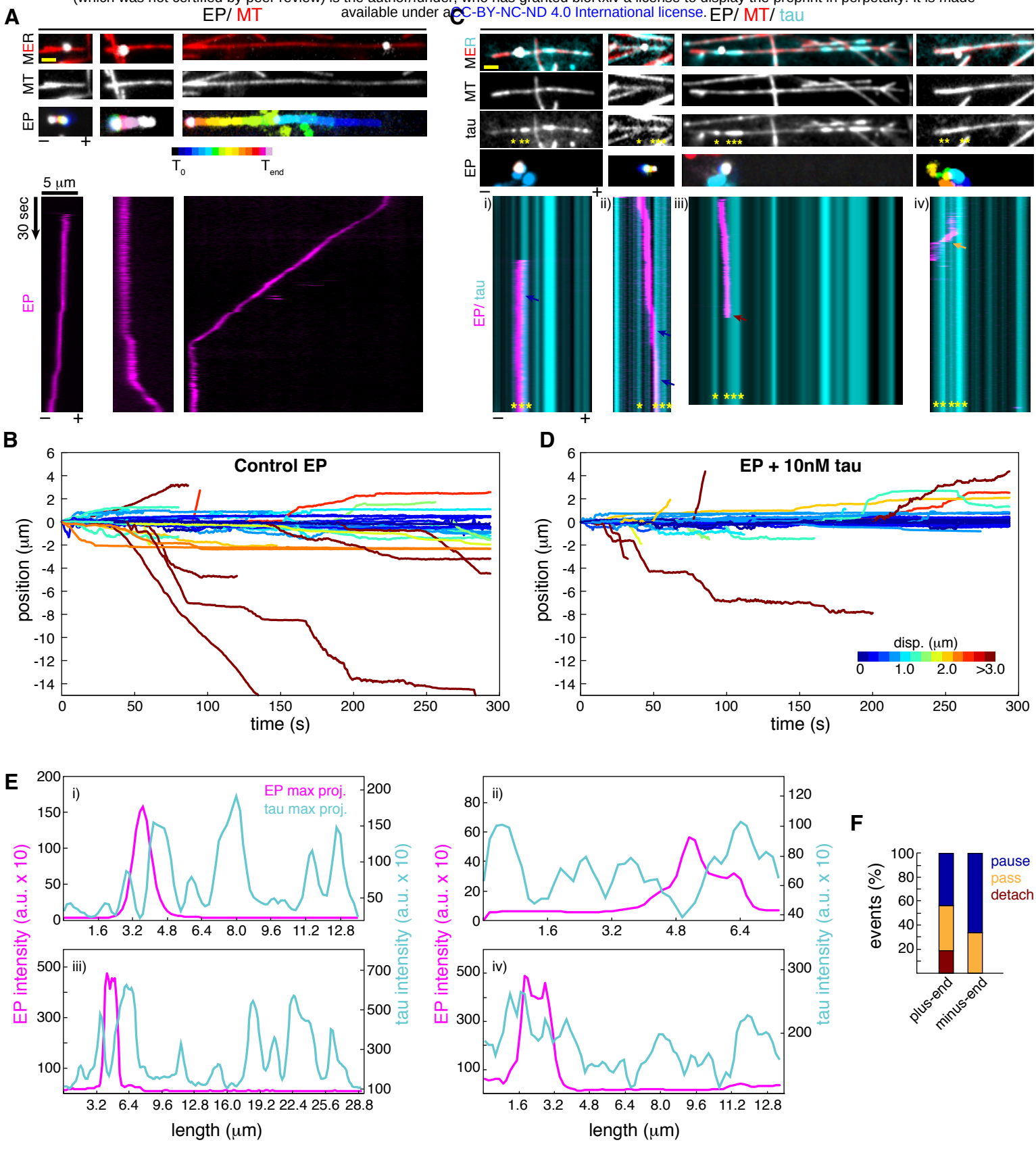

Figure 2

Figure 2) Tau reduces minus-end directed EP motility *in vitro*
A and C) Early phagosomes were extracted from cells and their motility was reconstituted *in vitro* along polarity marked microtubules (bright segment; minus-end) +/- 10 nM 3RS-tau. Images show microtubules (MT), tau, and max projections of EPs temporally color coded. Kymographs show examples of unidirectional plus-end and minus-end directed EPs +/- 10 nM tau. EPs often pause (*i* and *ii*: blue arrows), and less frequently pass through (*iv*; orange arrow) or detach from the microtubule (*iii*; red arrow) when they encounter tau patches (yellow asterisk). Scale bars are 2 μm or 5 μm for kymographs. **B and D)** Plots show trajectories of EPs directed towards the plus-end or minus-end of microtubules +/- tau (control; n = 55, 10 nM tau; n = 49). Trajectories are color coded by displacement. **E)** plots show linescans of the maximum projections of EP and tau fluorescence signals along microtubules from images *i–iv* shown in panel C. EP fluorescence intensity is shown on the left y-axis and tau fluorescence intensity is shown on the right y-axis. **F)** A bar graph shows the percentage of EPs that detach, pause, or pass-through tau patches (plus-end events; n = 16, minus-end events; n = 27).

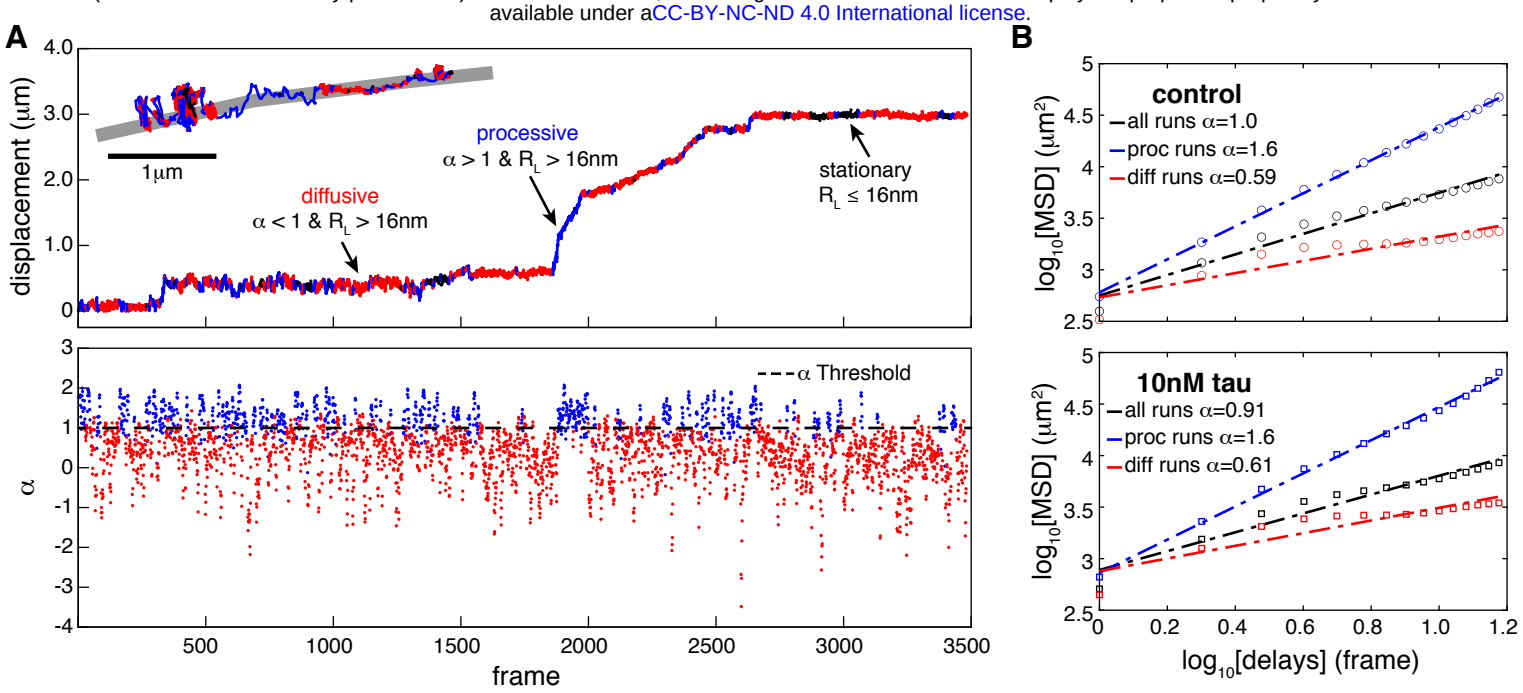

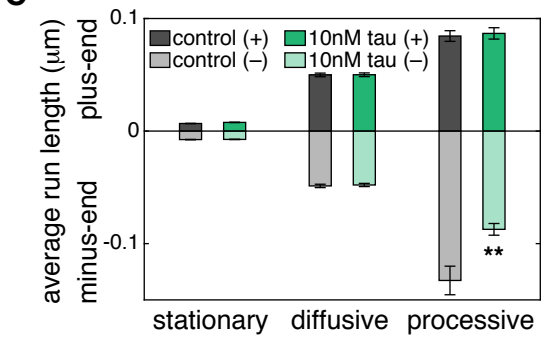

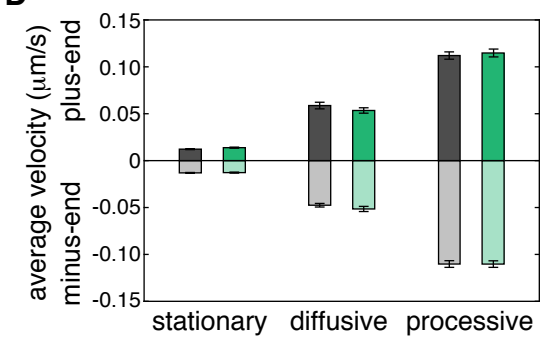

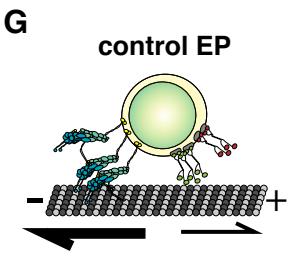

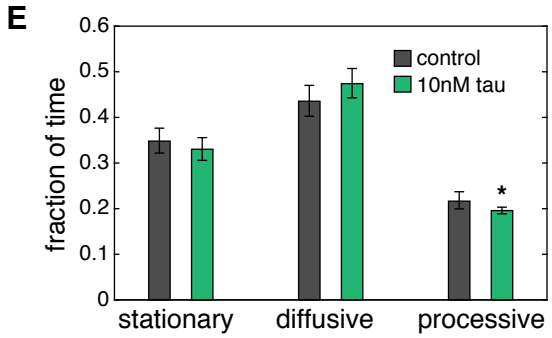

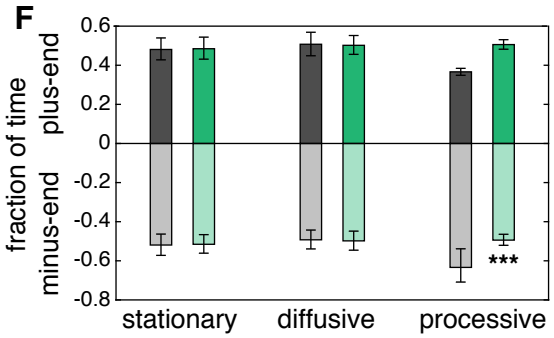

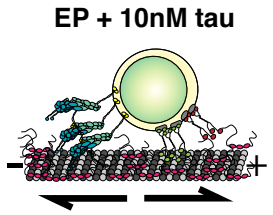

Figure 3

Figure 3) Change point analysis reveals that tau reduces EP minus-end directed processive transport

A) Plots show how change point analysis identified stationary (black), diffusive (red), and processive (blue) periods of motility for each trajectory (top graph) by calculating local alpha (α) values using a rolling MSD with a sliding window length of 12 frames (bottom graph). Change points occurred when the difference between two adjacent α-values was > 0.3. Stationary runs were identified as the period of motility between two change points with a run length (R_L) $\leq$ 16nm, which is the calculated mean tracking error (Fig. S3B), diffusive runs were categorized as runs with $R_L > 16$nm and $\alpha < 1$, and processive runs were categorized as runs with $R_L > 16$nm and $\alpha > 1$. The inset shows positional data from tracking an EP along a microtubule using FIESTA. The trajectory is colored to show periods of stationary, diffusive, and processive motility. Scale bar is 1 μm. **B)** The graphs show log-log MSD of EP transport following change point analysis. The α-values are shown for all runs, diffusive runs, and processive runs for control EPs (top) and EPs + tau (bottom). Bar graphs show **C)** the average run lengths and **D)** average velocities for stationary, diffusive, and processive runs identified by change point analysis +/- tau. Error bars show SEM, (** $p < 0.001$). **E)** A bar graph shows that tau does not significantly change the fraction of time of stationary and diffusive motility but slightly decreases processive motility. **F)** A bar graph shows the fraction of time of stationary, diffusive, and processive runs in the minus-end or plus-end direction +/- tau. While stationary and diffusive motility is directionally unbiased, 63.4% of processive motility is biased towards the minus-end of microtubules for control EPs, which is reduced to 49.4% in the presence of tau. Error bars in E and F show 95% confidence intervals (* $p < 0.05$, *** $p < 0.0001$). **G)** A cartoon schematic describes the impact of tau on EP motility. Control EPs are unidirectional and biased towards the microtubule minus-end (top). Tau reduces the run lengths and frequency of minus-end directed runs (bottom), which causes EP motility to shift to shorter runs with an equal fraction of plus-end and minus-end directed events.

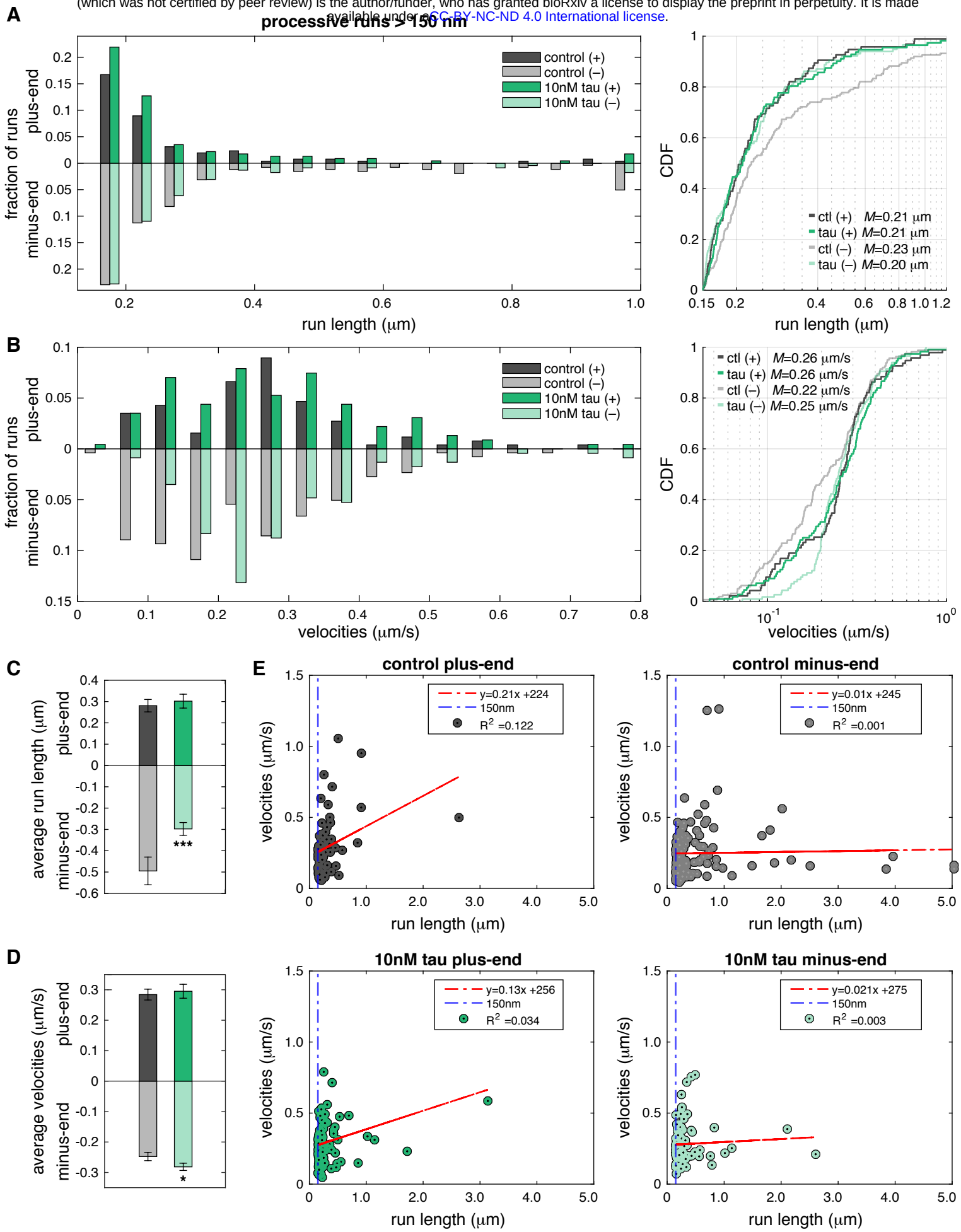

Figure 4

Figure 4) Tau strongly inhibits long-range minus-end directed processive runs
A) A histogram shows the distribution of run lengths for processive runs > 150 nm in the plus-end and minus-end direction +/- tau. Analysis of processive runs > 150 nm consisted of 95 plus-end and 162 minus-end control runs and 112 plus-end and 116 minus-end runs with tau. The cumulative distribution function (CDF) plot on the right shows that tau decreases the lengths of minus-end directed processive runs but does not impact plus-end directed runs (plus-end runs, not significant (n.s.); minus-end runs, $p < 0.05$). **B)** A histogram shows the distribution of velocities for processive runs > 150 nm in the plus-end and minus-end direction +/- tau. The CDF plot on the right shows that tau decreases the fraction of runs with slower velocities but has less impact on the fraction of runs with higher velocities or plus-end directed runs (plus-end runs, n.s.; minus-end runs, $p < 0.0001$). Median (*M*) run lengths and velocities are shown in A and B. Bar graphs show **C)** the average run lengths and **D)** average velocities for plus-end and minus-end directed processive runs > 150 nm +/- tau. Error bars indicate SEM, (* $p < 0.05$, *** $p < 0.0001$). **E)** Plots show velocities vs. run lengths of plus-end and minus-end directed processive runs for control (top) and + tau (bottom). Plots are fitted using a linear trend to show the proportionality of velocity and run length. Minus-end directed runs with low velocities and longer run lengths are more strongly inhibited by tau compared to shorter faster runs or plus-end directed runs.

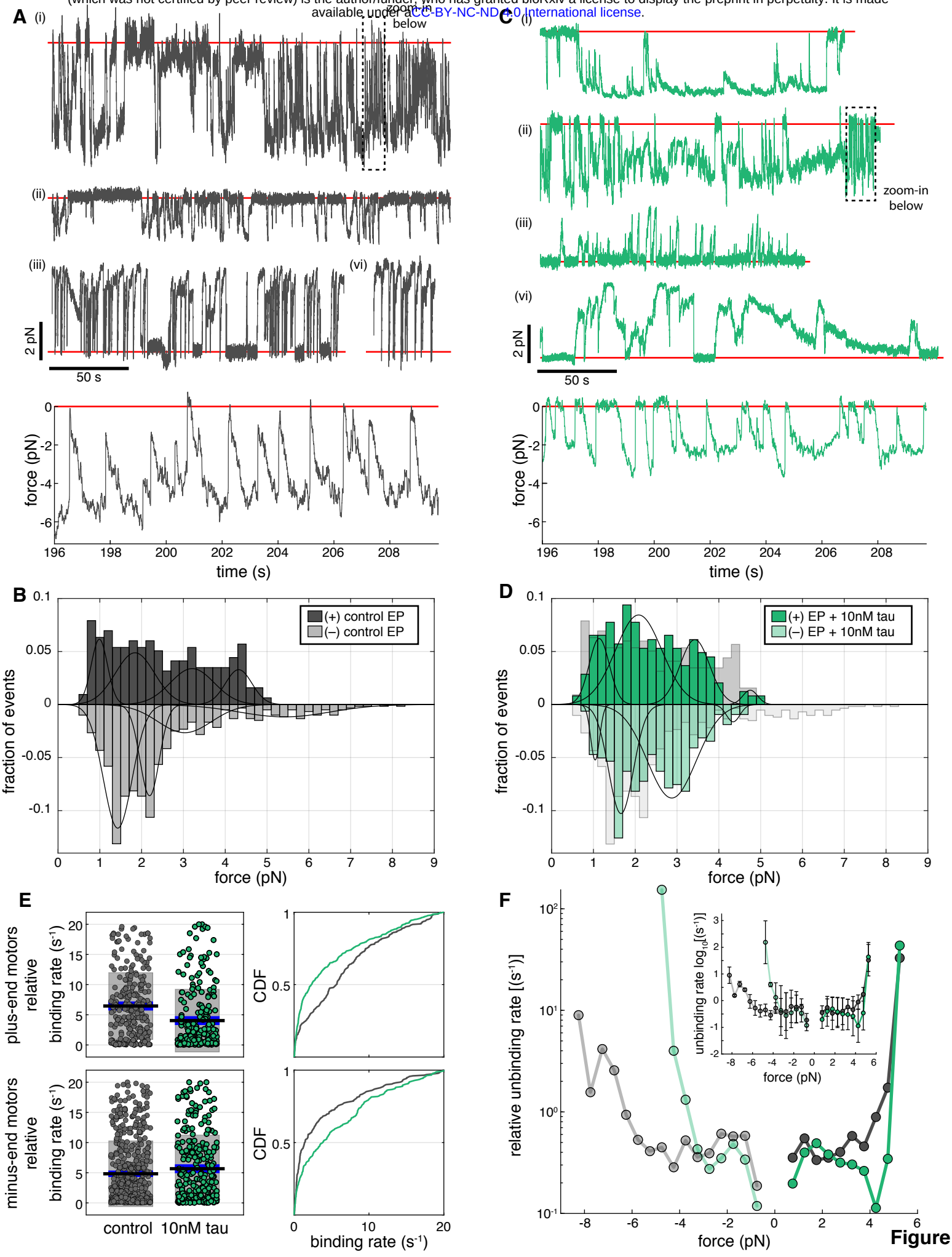

Figure 5

Figure 5) Tau reduces the forces generated by teams of multiple dynein transporting EPs A and C) Force traces of EPs +/- 10 nM tau were acquired at 2 kHz using an optical trap and median-filtered at 20 Hz. Force events were observed in both the minus-end direction (*i*, *ii*) and the plus-end direction (*iii*, *iv*) for A) control EPs (n = 904 events from 64 recordings taken over 11 independent experiments) and for C) EPs + tau (n = 563 events from 54 recordings over 11 experiments). Red lines show the trap center (0 pN). **B and D)** Histograms show the distribution of plus-end and minus-end force events with stall durations > 250 msec for B) control EPs and D) EPs + tau. Gaussian Mixture Model was used to describe the number of components within the distributions and the mean forces of each component. For control, mean peaks were identified at 1 pN, 1.9 pN, 3.2 pN, and 4.3 pN for plus-end forces and 1.4 pN, 2.2 pN, 3.1 pN and 5.5 pN for minus-end directed forces. In the presence of tau, mean peaks for plus-end directed forces are shown at 1.2 pN, 2.1 pN, 3.4 pN, and 4.6 pN, and minus-end directed forces show peaks at 1.0 pN, 1.7 pN, 2.9 pN, and 4.3 pN. Control EP force events were overlaid (light grey bars) on top of EP+ tau force events to show how tau reduces higher force events in both directions (plus-end forces, $p < 0.05$; minus-end forces, $p < 0.001$). **E)** Plots show the relative binding rates calculated for plus-end motors (top) and minus-end motors (bottom). On the right, CDF plots show how tau influences the fraction of the relative binding rates of plus-end and minus-end motors (plus-end motors, $p < 0.0001$; minus-end motors, $p < 0.05$). **F)** A plot shows the force-dependent relative unbinding rates of minus-end and plus-end directed forces +/- tau with stall times > 250 msec. The inset shows the log-unbinding rates on the y-axis. error bars indicate SEM.

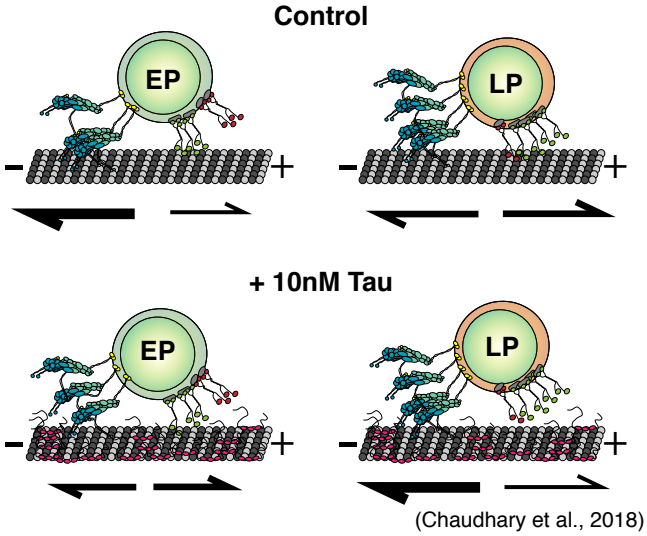

(Chaudhary et al., 2018)

Figure 6

Figure 6) Tau differentially regulates teams of motors transporting different cargoes
A cartoon schematic shows how EPs and LPs respond uniquely to tau on microtubules. While LPs are bidirectionally transported along microtubules, EPs exhibit unidirectional motility and more frequently move towards the minus-end of microtubules. Tau differentially impacts the motility of EPs and LPs. In the presence of tau, LPs are biased towards the minus-end of the microtubule, whereas the long-range minus-end directed transport of EPs is strongly inhibited.